AGU PUBLICATIONS

JGR

Journal of Geophysical Research: Oceans

RESEARCH ARTICLE

10.1002/2016JC011763

A process study of the Adriatic-Ionian System baroclinic dynamics

M. Reale[1,2,3], A. Crise[2], R. Farneti[3], and R. Mosetti[2]

[1]Department of Mathematics and Geosciences, Universita' di Trieste, Trieste, Italy, [2]OGS (Istituto Nazionale di Oceanografia e Geofisica Sperimentale), Borgo Grotta Gigante, Sgonico (TS), Italy, [3]Earth System Physics, International Centre for Theoretical Physics, Trieste, Italy

Key Points:
- Wind does not play a leading role in the vorticity and energy budgets of the Adriatic-Ionian System
- Reversals in the Ionian Sea take place only in the presence of an active boundary on the Aegean Sea/Levantine Basin side
- Reversals appear to be correlated with substantial exchanges of Availalble Potential Energy between Ionian and Aegean Sea

Correspondence to:
M. Reale,
reale.marco82@gmail.com

Citation:
Reale, M., A. Crise, R. Farneti, and R. Mosetti (2016), A process study of the Adriatic-Ionian System baroclinic dynamics, *J. Geophys. Res. Oceans*, *121*, 5872–5887, doi:10.1002/2016JC011763.

Received 29 FEB 2016
Accepted 28 JUN 2016
Accepted article online 4 JUL 2016
Published online 16 AUG 2016

Abstract The driving mechanisms behind the decadal reversal of the Ionian Sea upper layer circulation recently sparked a considerable discussion in the Mediterranean scientific community. It has been suggested that the reversal can be driven by variations in wind stress curl over the basin, baroclinic dynamics acting within the Adriatic-Ionian System (AISys) or baroclinic dynamics driven by thermohaline properties at the AISys eastern boundary. Here we perform numerical simulations in order to assess the relative importance of remote forcings (wind stress, thermohaline fluxes, thermohaline open boundary conditions) on the vorticity and energy budget of the Ionian Sea. A mechanistic understanding of the AISys dynamics is achieved with an approach based on an increasing complexity in the model forcings and domain. Our experiments suggest that wind stress does not play a leading role in the vorticity and energy budgets of the Ionian Sea. Wind stress can reinforce or weaken the circulation but it is not able to reverse its sign. Its role becomes dominant only in the absence of inflows through the Antikythira Strait and Cretan Passage. Instead, reversals in the upper layer circulation of the Ionian Sea take place only in the presence of an active boundary on the Aegean Sea/Levantine Basin side and appear to be correlated with substantial exchanges of Availalble Potential Energy between the two basins (as observed at the end of the Eastern Mediterranean Transient). From an energetic point of view, AISys can be explained therefore only if the role of the Aegean Sea is explicitly considered.

1. Introduction

The driving mechanisms behind the decadal reversal affecting the Ionian Sea upper layer circulation recently sparked a considerable and challenging discussion in the Mediterranean scientific community [*Korres et al.*, 2000; *Gacic et al.*, 2010; *Theocharis et al.*, 2014]. It has been suggested that the reversal can be driven by variations in wind stress curl over the basin [*Korres et al.*, 2000], baroclinic dynamics acting within the Adriatic-Ionian System (hereafter AISys, Figure 1a) [*Gacic et al.*, 2010] or baroclinic dynamics driven by thermohaline properties at the AISys eastern boundary [*Theocharis et al.*, 2014].

The physiography of the AISys and mechanisms suggested to explain the variability observed in the Ionian Sea upper layer circulation are now briefly discussed.

AISys consists of the Adriatic and the Ionian Seas connected by the Otranto strait (Figure 1a) and plays an important role in the Mediterranean Thermohaline circulation (MTHC) component in the Eastern Mediterranean Sea (EMED, for a complete list of acronyms used in the text see Table 1) [*Gacic et al.*, 2010]. The Adriatic Sea (Figure 1a) [*Mantziafou and Lascaratos*, 2004; *Gunduz et al.*, 2013] is an elongated basin (approximately 800 km long and 200 km wide) which is conventionally divided in three sub-basins: the northern Adriatic (NA) limited by the 100 m isobaths, the Middle Adriatic (MA), with a mean depth of about 140 m, extending up to the Palagruža Sill (170 m) and the southern Adriatic (SA) characterized by a deep pit (1200 m) and connected through the Otranto Strait (75 km wide and approximately 800 m deep) with the Ionian Sea [*Lipizer et al.*, 2014]. Both NA and SA are characterized by deep waters formation processes (DWF) which are favored by the cold and dry Bora wind flowing over the basin mainly in winter and the presence of Levantine Intermediate Water (LIW) which increases the potential for deep waters formation [*Mantziafou and Lascaratos*, 2004, 2008; *Gunduz et al.*, 2013] by adding saltier waters. A major part of deep waters (about 82%) are produced in the SA [*Mantziafou and Lascaratos*, 2004, 2008] through open-ocean convection processes [*Manca et al.*, 2002] and are mixed with those produced in the NA, forming the so-called Adriatic Deep Waters (hereafter ADW). ADW is characterized

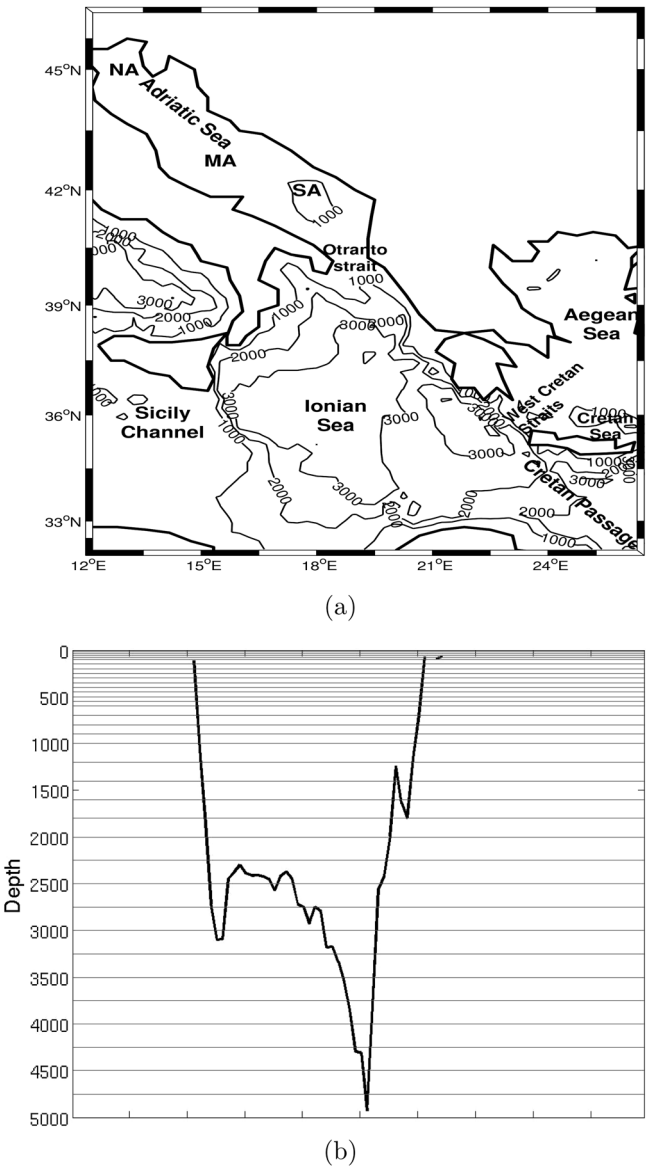

Figure 1. (a) The Adriatic-Ionian System (AISys) and relative bathymetry (in m) and (b) vertical levels spacing overlapped with the longitudinal profile of the AISys bathymetry at its deepest point.

by a temperature of T<13.3°C, a salinity S>38.68 and potential densities $\sigma_\theta \approx$ 29.17–29.18 kg m^{-3} [*Gacic et al.*, 2002] . ADW flows through Otranto Strait with an outflow ranging between 0.1 Sv (1 Sv=10^6 m^{3}s^{-1}) and 0.4 Sv [*Manca et al.*, 2002; *Mantziafou and Lascaratos*, 2004], ventilating the deep layers of Ionian Sea and the EMED.

The Ionian Sea is the deepest basin of the Mediterranean Sea (Figure 1a) [*Nittis et al.*, 1993]. It is connected through the Sicily channel (130 km wide and 300 m deep) with the Western Mediterranean, with the Cretan Sea through the West Cretan Straits [*Kontoyiannis et al.*, 1999; formed by the Kythira/Antikythira Strait and Elafonisos strait with a maximum depth of 700 m and ∼30 km width in correspondance of the Antikythira Strait) and with the Levantine Basin through the Cretan Passage (300 km wide and 2000 m deep) [*Nittis and Pinardi*, 1993]. The Ionian Sea represents a crossroad for the main kind of waters involved in the MTHC [*Gacic et al.*, 2010]. The Ionian deep layer is filled with the ADW, its intermediate layers are filled with LIW and CIW (Cretan Intermediate Water) [*Klein et al.*, 1999] while its surface layers are influenced by relatively fresher and colder Modified Atlantic water (AW) moving eastward and occasionally bifurcating northward entering the Southern Adriatic and leading to a decrease in the density of ADW [*Gacic et al.*, 2010].

A change of the MTHC component in EMED occurred during the 1990s when the main source of bottom waters for the basin shifted from the Adriatic to the Aegean Sea [*Roether et al.*, 1996; *Klein et al.*, 1999; *Lascaratos et al.*, 1999; *Roether et al.*, 2007]. This event has been called Eastern Mediterranean Transient (hereafter EMT) and it has been attributed mainly to meteorological anomalous conditions in the area and to changes in circulation patterns [*Roether et al.*, 1996; *Klein et al.*, 1999; *Lascaratos et al.*, 1999; *Roether et al.*, 2007]. During EMT the deep layers of EMED were filled with an inflow of 3 Sv (greater with respect to the Adriatic inflow) [*Roether et al.*, 2007] for 7 years, with waters of higher temperatures and salinity values (T>13.7°C, S > 38.8 and $\sigma_\theta \approx>$ 29.18 kg m^{-3}) with respect to those produced in the Adriatic Sea [*Klein et al.*, 1999].

EMT started in 1987 with the increase of densities of deep waters formed in the Aegean sub-basins as a consequence of an excessive winter cooling during the winters 1987, 1992, and 1993 [*Theocharis et al.*, 1999] that acted in addition to a previous salinity increase that took place between 1987 and 1991 [*Lascaratos et al.*, 1999; *Roether et al.*, 2007; *Beuvier et al.*, 2010; *Theocharis et al.*, 2014]. The principal outflow route for these dense waters was represented by the Kasos Strait and they started to affect the deep layers of EMED about 1990 with a peak in the delivering outflow around 1994 [*Roether et al.*, 2007; *Beuvier et al.*, 2010;

Table 1. Main Acronyms Used in the Text

Acronyms	Meaning
AISys	Adriatic-Ionian System
MTHC	Mediterranean Thermohaline circulation
EMED	Eastern Mediterranean
NA	Northern Adriatic
MA	Middle Adriatic
SA	Southern Adriatic
ADW	Adriatic Deep Water
LIW	Levantine Intermediate Water
AW	Modified Atlantic Water
CIW/CDW	Cretan Intermediate/Deep Water
NIG	Northern Ionian Gyre
EMT	Eastern Mediterranean Transient
BiOS	Bimodal Adriatic-Ionian Oscillating System

Theocharis et al., 2014]. The mean value of the outflow has been estimated to be around 3 Sv (mid 1992–1994) and the total amount was about twice the total volume of the Aegean Sea [*Roether et al*., 2007; *Sayin and Besiktepe*, 2010]. The Aegean contributions exiting the Kasos Strait propagated westward outflanking the Cretan Arc and quickly spread across the Ionian advected by its circulation (partly cyclonic along the periphery of the Ionian Sea) [*Roether et al*., 2007]. The EMT event started to relax from 1995 [*Theocharis et al*., 2002] and the outflow almost stopped in 1998 [*Klein et al*., 2000], although the densities in the Cretan Sea in 2001 were still high enough to sustain further outflow into the EMED [*Roether et al*., 2007].

Since 1997 the additional salinity supply into SA acts as favorable preconditioning for higher density DWF in this area. This would facilitate the ventilation of the bottom layers of the Ionian as before 1987 [*Klein et al*., 2000] despite recent evidences show that thermohaline properties in the Ionian are still far from those observed in the pre-EMT phase [*Cardin et al*., 2014].

The variability of the thermohaline circulation in the EMED was further argued as a consequence of the variability in the vorticity of the Northern Ionian Gyre (NIG) which has been observed periodically to reverse from anticyclonic to cyclonic and viceversa [*Gacic et al*., 2010; *Schroeder et al*., 2012; *Bessières et al*., 2013]. This decadal oscillation affecting the spreading of the AW eastward and LIW westward in the AISys, is able to influence the salinity in the Eastern Basin [*Gacic et al*., 2011], in the Sicily channel [*Gacic et al*., 2013] and the advection of nutrients and salt in the Adriatic Sea [*Civitarese et al*., 2010; *Gacic et al*., 2010].

The variability observed in the Ionian circulation has been often associated with a change in the wind stress curl over the area [*Pinardi et al*., 1997; *Korres et al*., 2000; *Demirov and Pinardi*, 2002; *Molchard et al*., 2002] while, recently, this variability has been explained in terms of the Bimodal Adriatic-Ionian Oscillating System (hereafter BiOS). BiOS is a feedback mechanism linking the Ionian and Adriatic according to the following characteristics [*Gacic et al*., 2010]: (a) AISys behaves as a bimodal oscillating system; (b) When a cyclonic circulation is present in the north Ionian Sea, salty LIW enters in the Adriatic leading to an ADW production of increasing density which determines a shallowing of isopycnal surfaces in the Ionian. The resulting squeezing of water column produces a reversal of the circulation from cyclonic to anticyclonic conditions; (c) When an anticyclonic circulation is present in the north Ionian, AW is deflected in the Adriatic leading to production of ADW of lower density which spreads in the Ionian Sea producing a deepening of isopycnal surfaces in the Ionian. The resulting stretching of the water column results in a reversal of circulation from anticyclonic to cyclonic conditions.

This mechanism suggests that internal processes are able to sustain the variability of the circulation in the Ionian independently from external forcings such as wind [*Gacic et al*., 2010] . After a first transition from an anticyclonic to a cyclonic mode observed during 1997 [*Borzelli et al*., 2009] altimetric maps have shown a new anticyclonic mode starting in 2006 [*Gacic et al*., 2010; *Bessières et al*., 2013]. The cyclonic mode started in 2011 and unexpectedly ended in 2012 when a new reversal to anticyclonic conditions was observed [*Gacic et al*., 2014]. This premature inversion has been attributed to the extremely strong winter in 2012, which caused the formation of very dense ADW, flooding the Ionian flanks in May and inverting the bottom pressure gradient [*Gacic et al*., 2014]. The 2012 inversion has only been temporary and the circulation mode changed again to cyclonic at the beginning of 2013 [*Gacic et al*., 2014].

Recently, *Theocharis et al*. [2014] suggested that the decadal variability observed in the Ionian circulation reflects an internal mechanism driving the alternation of the Adriatic Sea and the Aegean Sea as main DWF sites for the EMED. In particular, *Theocharis et al*. [2014] and *Velaoras et al*. [2014] observed that when the Adriatic Sea acts as DWF site for the EMED, AW are deflected northward in order to balance the outflow of ADW through the Otranto Strait. AW entering the SA leads to a decrease in salinity and, consequently, of the potential for DWF. At the same time this deflection together with the recirculation of LIW in the

Levantine basin leads to an increase of salinity in the Aegean Sea and, thus, of the potential for DWF with the final result to shift the DWF from the Adriatic Sea to the Aegean Sea. On the contrary, when the Aegean Sea acts as DWF site for the EMED, AW are deflected eastward in order to balance the outflow of dense water masses through the West Cretan Straits and Cretan Passage. AW entering the Aegean Sea/Cretan Passage leads to a decrease in salinity and, consequently, of the potential for DWF. At the same time this deflection of AW leads to an increase of salinity in the Adriatic Sea and, thus, of the potential for DWF with the final result to shift back the DWF from the Aegean Sea to the Adriatic Sea. This thermohaline pumping [*Theocharis et al*., 2014; *Velaoras et al*., 2014] involves the whole thermohaline cell of EMED and not only the Adriatic-Ionian Sea as in the BiOS hypothesis [*Gacic et al*., 2010]. In both cases the role of long term atmospheric forcings is not dominant in driving the circulation reversals. The signature of this thermohaline pumping is evident on the upper-intermediate waters of the Ionian and Levantine basin and Aegean Sea which show an almost anticorrelated decadal oscillation behavior [*Krokos et al*., 2014]. A similar anticorrelated oscillation has been observed between the Adriatic and Aegean Seas [*Bensi et al*., 2016]

The aim of this study is to provide a deeper insight into the dynamics of the AISys through a modeling approach in order to assess the relative impact of the external forcing and internal processes acting on the AISys by evaluating their effects on the vorticity and energy budgets. A process study based on a series of numerical experiments has been conceived by setting up an idealized model for the AISys. The physics and forcings of the model have been progressively refined in order to rank the relevant mechanisms acting on the variability observed in the Ionian circulation, quantifying the contribution of the external forcing (wind in this study) to the Ionian circulation, and assess the vorticity and energy balance within the Ionian basin.

This paper is organized as follows: in section 2 we provide the description of the settings of the numerical model and the forcings used and in section 3 we describe the analysis of the vorticity and energy budget for the Ionian basin. We summarize our main conclusions in section 4. Appendix A provides a description of the numerical model MITgcm. Appendix B describes the vorticity and kinetic energy budget.

2. Data and Methods

The dynamics of the AISys has been simulated through the primitive equations model MITgcm (MIT general circulation model) [*Adcroft et al*., 1997; *Marshall et al*., 1997a,1997b].

The model is described in Appendix A. In the following sections we outline the main configuration, parameters and forcings of the model that have been used to simulate the dynamics of the AISys.

2.1. Domain of Integration

The model's bathymetry was derived from the Mediterranean Forecast System [*Oddo et al*., 2009]. The original high resolution bathymetry (dX=dY=0.0625°) was interpolated to a lower resolution (dX=dY=0.125°, Table 2). The domain extends over 108 × 100 points, approximately between 12.875E and 25E and 30.18N to 42.75N (Table 2). The domain does not include the NA and the MA. The new interpolated bathymetry has been further modified in two distinct configurations: one with closed and one with open boundaries. The first experiment, CLWIND, is characterized by closed boundary conditions at Sicily Channel, Cretan Sea and Cretan Passage. The second experiment, OPWIND, is similar to the interpolated original bathymetry with the only difference that the Cretan Sea has been imposed at the end of a channel obtained iterating eastward ten times the Antikythira strait bathymetry (from now on the three boundaries in our domain will be indicated as Sicily Channel, Antikythira Strait and Cretan Passage). The model has 36 levels (Table 2 and Figure 1b; delZ) with an inhomogenous distribution (from 20 m in the first 100 m to 250 m in the last 1000 m).

Table 2. Main Parameters Used in All Experiments

Parameter	Description	Values
dX, dY	Horizontal grid spacing	0.125°
dZ	Number of levels	36
(λ, φ)	Domain size	12.875E–25E; 30.1875N–42.75N
A_h, A_T, A_S	Horizontal eddy diffusivity coefficient for Momentum, Temperature, Salinity	100
A_{hz}, A_{Tz}, A_{Sz}	Vertical eddy diffusivity coefficient for Momentum, Temperature, Salinity	10^{-4}

2.2. Model Configuration

The model has been run in hydrostatic configuration. Linear free surface has been used as parametrization for

the upper boundary. The grid chosen for the numerical experiments is Spherical Polar. The numerical simulations cover the period 1987–2008.

The model used (Table 2) a constant horizontal eddy diffusivity for momentum, temperature and salinity (100 m^2s^{-1} for all the experiments). Based on our previous modeling experience in the target area, the model employs the K-profile Parametrization for vertical mixing (KPP) [*Large et al.*,1994] with an initial value of vertical viscosity of 10^{-4} m^2s^{-1} for momentum, temperature and salinity (Table 2). KPP is able to deal with different processes involved in the mixing of interior such as internal wave activity and/or shear instability [*Large et al.*, 1994]. For the advection of a passive tracer a third order DST (direct space-time) scheme with flux limiter has been employed in order to guarantee the numerical stability of runs and to avoid anomalous advection of tracers [*Querin et al.*, 2006].

2.3. Boundary Conditions (BC)

Zonal and meridional components of wind speed, which are prescribed as surface conditions, are obtained from an atmospheric model simulation carried out in the Med-Cordex domain [*Giorgi et al.*, 2012]. The 3 hourly data with a resolution of 12 km are available for the period 1979–2010. The area corresponding approximately to the AISys has been extracted from the data set and then interpolated over a regular longitude-latitude grid. Figure 2a shows the observed variation of vorticity induced by the wind stress over the Ionian Sea for the period 1987–2010. The wind stress curl is mainly anticyclonic (the input of vorticity will be analyzed in the next sections) and exhibits a seasonal cycle with a positive peak in winter reflecting the cyclone tracks crossing the area (not shown here). However the mean wind vorticity input is not spatially homogenous . The northern part of the basin is characterized by a predominat cyclonic wind stress input, whereas the southern part is dominated by an anticyclonic input.

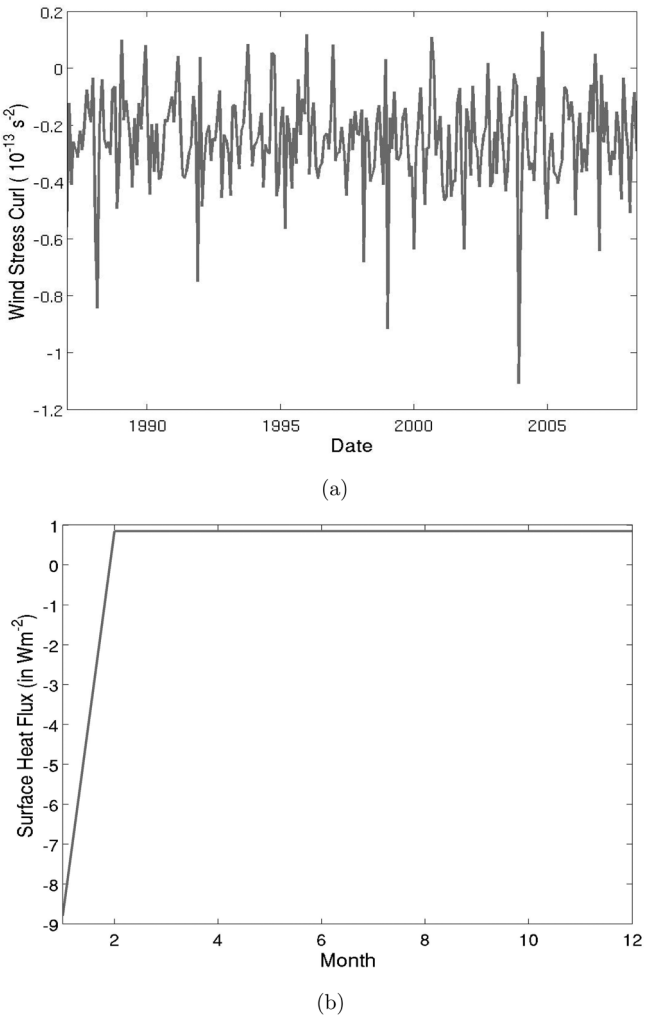

Figure 2. (a) Mean Monthly wind stress curl over the Ionian Sea in the period 1987–2010 (in s^{-2}) and (b) the annual cycle of the mean surface heat flux over the domain (in W m^{-2}).

Zonal and meridional components of ocean current, which have been prescribed at the lateral boundaries of the domain, have been derived from the MyOcean data set (www.myocean.eu). MyOcean is an reanalysis originating from the simulations of Mediterranean Forecasting System based on the NEMO model [*Oddo et al.*, 2009]. NEMO has been implemented on the Mediterranean domain with a horizontal spatial resolution of 1/16 and 72 unevenly spaced vertical levels [*Oddo et al.*, 2009]. Data have a monthly resolution, covering the period 1987–2012 and have been interpolated into our spatial horizontal and vertical resolutions. Data have been further corrected in order to balance the inflow and outflow through the boundaries. A sponge layer algorithm has been applied to both boundaries in order to ensure the numerical stability of our model. In the sponge layer (of 10 grid point

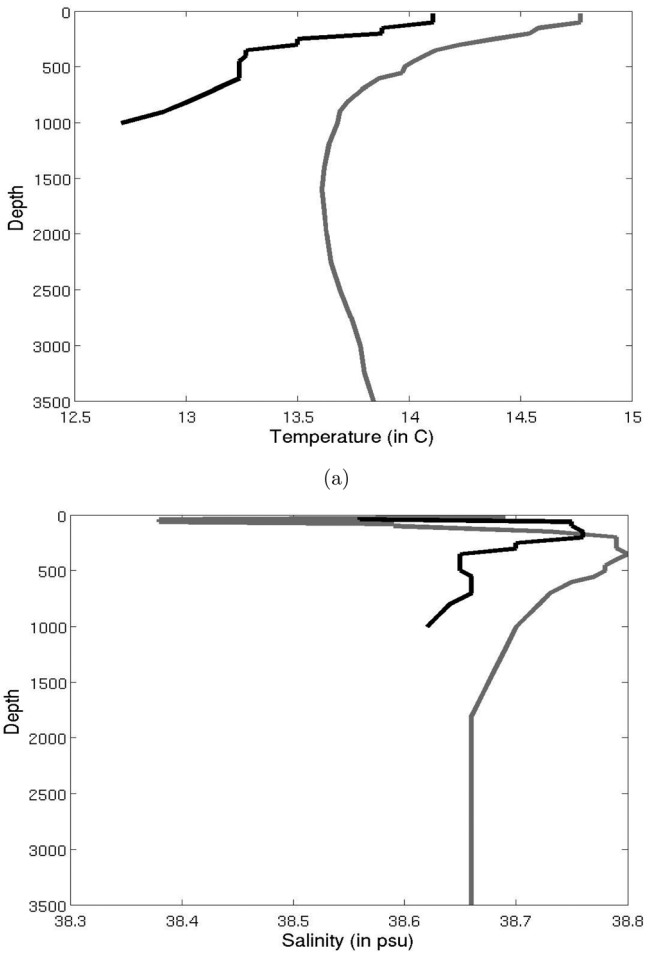

Figure 3. Vertical profiles of (a) Temperature and (b) Salinity in 1987 in the Adriatic (black line) and Ionian Sea (grey line).

width) both velocity components in each cell of each vertical level are a weighted average between the velocity of the innermost point of the sponge layer and the velocity of the corresponding open boundary cell [*Querin et al.*, 2006]. The weight is defined by the distance from the boundary. The velocities in the inner grid points are relaxed to these prescribed values within a 5 days^{-1} time period.

Temperature and Salinity vertical profiles, prescribed as boundary conditions at the two lateral boundaries, have been derived from NEMOMED8 experiment, the configuration for the Mediterranean area (MED) of NEMO ocean model [*Beuvier et al.*, 2010; *Herrmann et al.*, 2010]. It covers the whole MED and is forced by ARPERA daily mean fields of momentum, freshwater and heat flux [*Beuvier et al.*, 2010; *Herrmann et al.*, 2010]. The experiment covers the period 1960–2008 and has especially been designed to model the factors triggering the EMT [*Beuvier et al.*, 2010; *Herrmann et al.*, 2010]. An averaged annual profile has been computed for each area corresponding to Sicily Channel, Cretan Sea and Cretan Passage and applied to each of our boundaries for each year of the simulation.

The model is forced at the surface by an artificial heat flux (AHF, Figure 2b). Area, intensity and periodicity of this artificial flux have been chosen in order to properly reproduce the DWF in the SA, to guarantee a reasonable value of ADW outflow at Otranto Strait and to obtain realistic thermohaline ADW properties even in absence of the dense water contribution coming from NA (not included in the model domain). To ensure the thermal balance at the surface of the domain an appropriate slightly positive heat flux is imposed over the basin for the rest of the year. Several tests have been carried out to check the capability of AHF to reproduce the DWF in the SA. Our experiments have shown a good agreement of the simulated values of volume/outflow of ADW through the Otranto with those reported in the scientific literature [*Gacic et al.*, 2002]. The model has been able, indeed, to capture the variability in DWF in the SA. Hence, despite its relative

Table 3. Main Characteristics of CLWIND and OPWIND Experiments

Name	IC	Boundaries	BC
CLWIND	Modified Roether conditions (MRC)	Closed (CL)	• Wind Regcm4 1987–2010 • AHF
OPWIND	Modified Roether Conditions (MRC)	Open (OP)	• Wind Regcm4 1987–2010 • MyOcean 1987–2012 • NemoMed8 1987–2008 • AHF

semplicity and temporal homogeneity, AHF has been able to induce a realistic physical picture. Figure 2b shows the annual cycle of AHF over the domain. The annual cycle has been employed as perpetual year for the entire lenght of simulation.

No evaporation-precipitation-runoff forcing has been considered. Additional boundary conditions (for all experiments) are no slip conditions for both momentum and tracers at the solid boundaries. Due to the coarse vertical resolution of the experiments free slip conditions on the bottom is imposed.

2.4. Initial Conditions

Temperature and salinity initial conditions are the same for all the experiments and have been derived initially from temperature and salinity profiles recovered in the Ionian and Adriatic Sea during the German crusie M5/6 in 1987 [*Roether et al.*, 2007; W. Roether, 2014). An averaged profile for both temperature and salinity has been computed separately for both the Adriatic and the Ionian Sea (Figures 3a and 3b) and applied entirely to each area in our domain. In order to avoid any sharp gradient in both temperature and salinity a buffer zone between the two areas of 10 grid points with a linear variation of temperature and salinity has been established. In both closed and open boundary configurations the model has been run for a period of 20 years using 1987 data as forcings (wind, heat fluxes, MyOcean data, NemoMed data). The resulting temperature and salinity 3-D fields (hereafter Modified Roether conditions, MRC) have been used as final initial conditions for our experiments. Initial velocity is zero all over the domain.

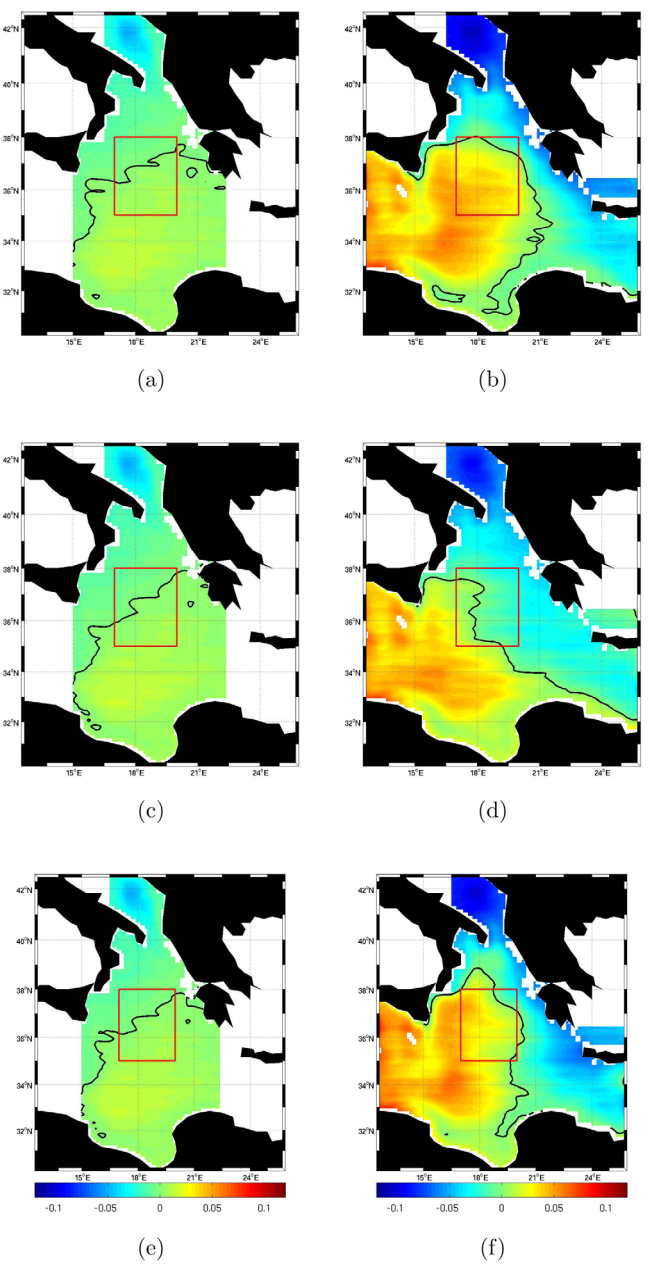

Figure 4. Mean SSH (in m) in (a, c, e) CLWIND and (b, d, f) OPWIND in the period (a, b) 1993–1997, (c, d) 1998–2005, (e, f) 2006–2008. Red rectangle points out the area of NIG. Black thin line represents the level zero for the SSH.

Table 3 shows the main characteristics of the two experiments that will be considered in our study, CLWIND and OPWIND. The period of the analysis for both experiments is 1987–2008. The outputs are 30 day averaged fields.

3. Results

3.1. AISys Circulation in the Period 1987–2008: Sensitivity Experiments

In CLWIND (Figure 4a, 4c, and 4e) in the three periods of the analysis the Ionian Sea is characterized by a permanent negative (positive) anomaly in its northern (southern) part corresponding to a cyclonic (anticyclonic) circulation respectively [*Molchard et al.*, 2002; *Borzelli et al.*, 2009]. This spatial pattern reflects the wind curl spatial variability as pointed out in the previous section (see also the next section for the vorticity budget analysis). In the case of OPWIND (Figures 4b, 4d, and 4f)

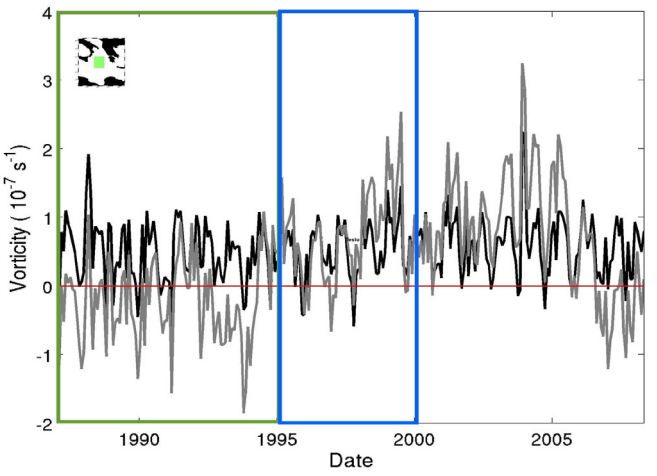

Figure 5. Monthly averaged Z3 (in s-1) in the first 500 m of Ionian for the period 1987–2008 in the experiment CLWIND (black line) and OPWIND (gray line). Red line represents the level zero for the Z3. Green Rectangle represents the EMT period, the blue the post EMT phase.

the period 1993–1997 (Figure 4b) is characterized by a permanent positive SSH anomaly (anticyclonic circulation) occupying the Ionian [*Borzelli et al*., 2009; *Gacic et al*., 2010, *Bessières et al*., 2013] whereas in the 1998–2005 (Figure 4d) the Ionian Sea is mostly filled by the negative SSH anomaly (cyclonic circulation) with a positive anomaly limited to the southern basin and Sicily Strait [*Borzelli et al*., 2009; *Gacic et al*., 2010; *Bessières et al*., 2013]. Finally, the period 2006–2008 (Figure 4f) in OPWIND is characterized by a new positive anomaly (corresponding to an anticyclonic pattern) occupying the whole basin [*Gacic et al*., 2010; *Theocharis et al*., 2014]. The negative values of SSH observed along the eastern flank of the Ionian in the period 1993–1997 (Figure 4b) is due to the spreading of Aegean Waters (CDW) during the EMT [*Roether et al*., 2007; *Borzelli et al*., 2009] and has been observed in the OPWIND experiment using a passive tracer released in the Antikythira strait (not shown here).

In both experiments the southern Ionian Sea exhibits a permanent SSH positive anomaly. The same anomaly has been observed in the case of an experiment with closed boundaries forced only by AHF (not shown) .This SSH anomaly appears to be, indeed, a permanent feature of the Ionian circulation eventually reinforced by the wind.

Figure 5 shows the monthly mean volume-averaged relative vorticity (Z3) in the first 500 m in the Northern Ionian (the green square in the small map in Figure 5) for OPWIND (gray line) and CLWIND (black line). CLWIND shows a permanent cyclonic circulation, while the circulation in OPWIND is characterized by two reversals. The circulation is anticyclonic in the period 1993–1997, particularly strong in 1993–1995 which corresponds to the peak of EMT [*Roether et al*., 2007; *Borzelli et al*., 2009; *Beuvier et al*., 2010; *Gacic et al*., 2010; *Theocharis et al*., 2014] and soon after the end of the EMT the circulation switches to cyclonic, stronger than in the CLWIND case. Then after the 2005 the circulation reverses to anticyclonic.

Figure 6a shows the Hovmoeller diagram of vorticity in the Ionian Sea in the case of OPWIND. The variability is limited to the first 500 m and the signal on the bottom is generally cyclonic due to the filling with ADW or CDW. In general the structure of vorticity in the Ionian Sea can be described as a bi-layer [*Gacic et al*., 2010] with zero level for vorticity located around 500 m. This result fits well with the structure of the Ionian Sea as predicted by a quasi–geostrophic model described by F. Crisciani and R. Mosetti (personal communication, 2015). Variations in the bi-layer structure, mainly between 2000 m and 3000 m, are likely to be linked to the formation of ri-circulation areas due to the topography (observed in some maps, not shown here).

Figure 6b shows the Hovmoeller diagram of potential density in the SA for OPWIND. In particular it is clear how the cyclonic phase is associated with an increase in the convection depth which ends with the beginning of an anticyclonic phase in the 2006, characterized conversely by a decrease in the convection depth itself . This variability cannot be explained in term of neither AHF (as it exhibits the same characteristics throughout the experiments) neither to evaporation/precipitation/runoff variability (as they are not included in our experiments) . This variability can be explained in term of an enhanced advection of AW (LIW) in the SA in correspondance of anticyclonic (cyclonic) pattern in the Ionian Sea [*Gacic et al*., 2010]. During an cyclonic (anticyclonic) pattern LIW (AW) are advected in the SA leading to an increase (decrease) in the potential of deep waters formation and convection [*Gacic et al*., 2010].

Figure 7 shows the total Kinetic Energy (KE, gray line) and Quasi-Geostrophic Avalaible Potential Energy (hereafter APE_{QG}) [*Huang*, 2005; *Korres et al*., 2000; *Brown et al*., 2011] (black line) of the Ionian Sea in the experiment CLWIND (a) and OPWIND (b). In CLWIND, the KE and APE_{QG} behavior is similar and mean values of the two

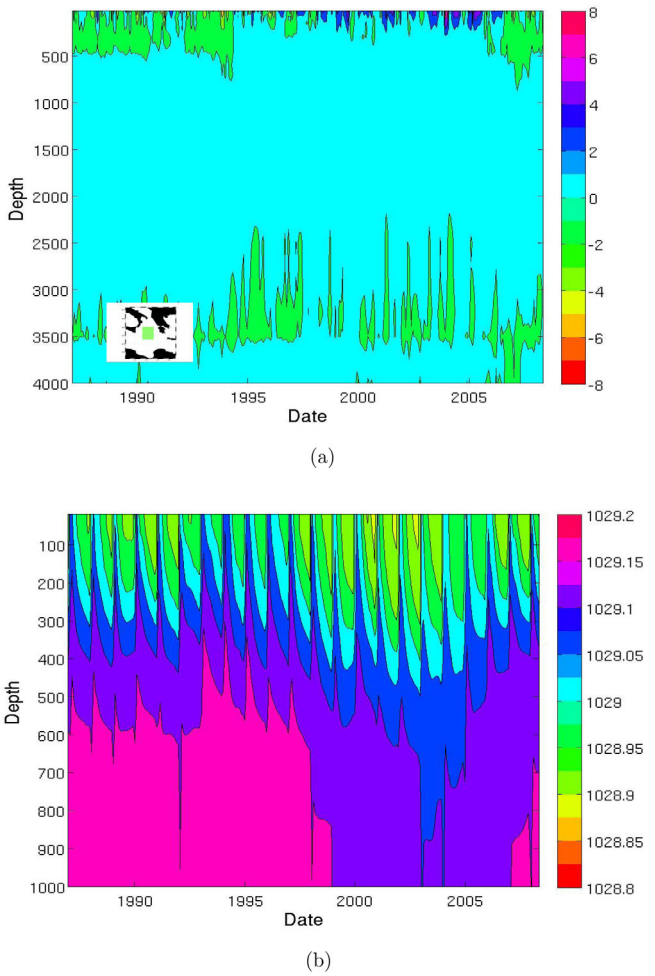

Figure 6. Hovmoller diagram of (a) monthly averagd vorticity (in 10^{-7} s^{-1}) in the Ionian Sea and (b) monthly averaged potential density in the SA (in kgm^{-3}) for the period 1987–2008 in OPWIND.

quantities are $1.5 \times 10^{14}J \pm 0.58 \times 10^{14}J$ and $4.2 \times 10^{15}J \pm 0.92 \times 10^{15}J$. In OPWIND the mean values of KE and APE_{QG} are respectively $4.5 \times 10^{14}J \pm 1.58 \times 10^{14}J$ and $7.9 \times 10^{16}J \pm 3.3 \times 10^{16}J$. Using the ratio $APE_{QG}/KE = L^2/R^2$ with L the scale of basin (zonal) and R the internal radius of deformation [*Gill et al.*, 1974] we have $L^2/R^2 = O(100)$. Hence, the length scale is much larger than the mesoscale eddy scale and energy is primarily in the form of potential energy.

The high values of standard deviation observed in both KE and APE_{QG} (OPWIND) reflect the different energetic level of the Ionian Sea corresponding to different circulation states. The anticyclonic state during the EMT corresponds to a high value of KE in the system and a minimum value for APE_{QG}. The cyclonic state between 1997 and 2005 corresponds to a maximum in both KE and APE_{QG}. The new anticyclonic pattern in 2006–2008 corresponds again to a minimum for APE_{QG} and a high value of KE.

3.2. Analysis of the Mechanisms Driving the Variability in the AISys Circulation

In order to identify the possible mechanisms driving the variability in the upper layer circulation of the Ionian Sea we carried out an analysis of the (relative) vorticity and kinetic energy budget in the Ionian. In Appendix B we report the definition and the numerical computation of both budgets.

In general, it is not straigthforward to interpret the results of both budgets in terms of source(s) and sink(s). For example the surface pressure gradient vorticity input can be influenced by wind stress through Ekman pumping but at the same time by the spreading of deep waters along the flanks of the basin. The same can happen to the baroclinicity as wind stress may induce vertical displacement of the isopycnals and so altering the horizontal density gradient. Also, the same baroclinicity may be influenced by stretching of water column as this may influence the vertical displacement of the isopycnals. We will thus focus our attention only on a few terms, considering those that have been previously analyzed and deemed to be the main factors affecting both budgets: the wind input and the stretching term for the vorticity budget [*Gacic et al.*, 2010], and the wind input and the conversion from APE_{QG} to KE for the kinetic energy budget [*Korres et al.*, 2000].

3.2.1. CLWIND

In CLWIND, the vorticity input from the wind is approximately seven times greater than the lateral flux through the Otranto strait (-38.57 ± 21.82 m^3s^{-2} and 5.66 ± 2.97 m^3s^{-2}, respectively). As previously noted, our definition of vorticity flux does not allow us to identify the sign of vorticity input (although we know, from experiments performed without wind forcing, that the input of vorticity from Otranto is anticyclonic). The stretching term is equal to -29.18 ± 22.46 m^3s^{-2}, weaker than the wind input. We deduce that internal mechanisms linked to the outflow of ADW through the Otranto strait do not play a leading role in determining the variability of the vorticity in the Ionian Sea.

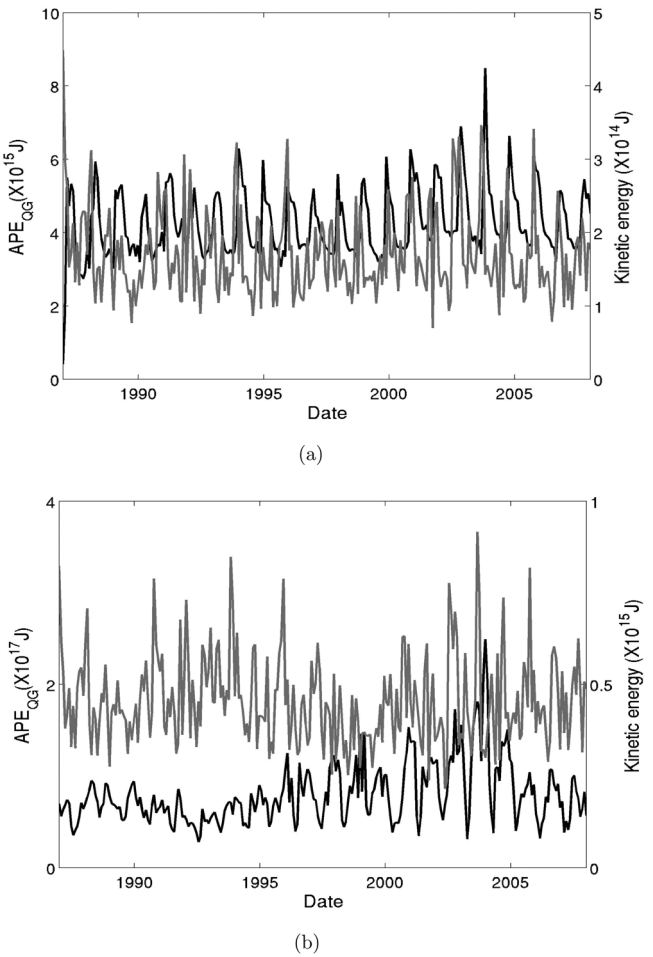

Figure 7. Monthly Total Kinetic energy (in J, gray line) and APE_{QG} (in J, black line) in the Ionian for the period 1987–2008 in (a) CLWIND and (b) OPWIND.

The input of kinetic energy from the wind into the Ionian Sea is two order of magnitude greater than the corresponding kinetic energy input through the Otranto Strait ($8.56 \times 10^{17} \pm 6.19 \times 10^{17}$ Wm^3 and $-6.12 \times 10^{15} \pm 5.91 \times 10^{15}$ Wm^3 respectively). The Ionian Sea imports from the SA APE_{QG} ($-2.18 \times 10^{17} \pm 4.19 \times 10^{17}$ Wm^3) which, as shown by the high standard deviation, shows periodic inversions of the flux, probably linked to the periodicity of the forcing acting on SA.

Part of the total kinetic energy is dissipated through horizontal and vertical dissipation (not shown) and the rest ($-2.71 \times 10^{17} \pm 5.36 \times 10^{17}$ Wm^3) is transferred to the reservoir of APE_{QG} through the vertical displacement of the isopycnals induced by the wind [*Brown et al*., 2011] and, probably to a less extent, by vortex stretching (in this framework it is not possible to separate the two mechanisms).

This may explain the similar behavior (Figure 7a) exhibited by APE_{QG} and KE (we are not considering in the APE_{QG} the buoyancy fluxes at surface as they are constant throughout the simulation). The conversion term exhibits a high standard deviation so occasionally (not shown here) the flux from KE to APE_{QG} inverts its sign in response to variations in the wind stress curl over the basin (the forcing on the SA is always the same in our experiments and so it cannot affect the hydrostatic pressure gradient).

Given the results from the experiment CLWIND we conclude that the wind is the main mechanism driving the vorticity and kinetic energy variability in a closed AISys.

3.2.2. OPWIND

In this section we analyze the vorticity and kinetic energy budgets for the Ionian Sea in the case of lateral open boundaries (OPWIND). Table 4 shows the mean flux of vorticity in the period 1987–2008 from the wind, through the Sicily Channel, the Antikythira Strait, the Otranto Strait and the Cretan passage. With respect to CLWIND it is evident that exchanges of vorticity with nearby basins are comparable with the wind input. In particular, the Sicily channel is the most important source of vorticity through the AW inflow despite its influence due to the geostrophic adjustment is likely to be limited to the southern part of the basin. Exchanges of vorticity with Antikythira Strait are greater than those with the Otranto Strait. Particularly relevant is the high standard deviation for the flux of vorticity through the Antikythira strait, which exhibits a strong peak (not shown here) in correspondance to the EMT event.

Table 4. Flux of Vorticity (m^3s^{-2}) and KE ($W\ m^3$) From the Wind, Sicily Channel, Antikythira Strait, Otranto Strait and Cretan Passage in the Period 1987–2008

	Vorticity (m^3s^{-2})	KE ($W\ m^3$)
Wind	-35.62 ± 21.49	$1.80 \times 10^{18} \pm 1.10 \times 10^{18}$
Sicily Channel	-44.61 ± 23.49	$4.41 \times 10^{16} \pm 4.03 \times 10^{16}$
Otranto strait	2.41 ± 1.34	$1.52 \times 10^{15} \pm 1.86 \times 10^{15}$
Cretan Passage	-18.91 ± 12.78	$3.83 \times 10^{16} \pm 3.80 \times 10^{16}$
Antikythira strait	-9.56 ± 10.69	$-7.83 \times 10^{16} \pm 1.38 \times 10^{17}$

Table 5. Flux of Vorticity (m^3s^{-2}), From the Wind, Stretching Term (in the First 500 m), Antikythira Strait, Otranto Strait, and Cretan Passage in the Period 1993–1997, 1998–2005, and 2006–2008

	Wind	Stretching	Cretan Passage	Antikythira Strait	Otranto Strait
1993–1997	-33.52 ± 20.29	-101.7 ± 35.65	-15.26 ± 10.28	-16.45 ± 20.39	2.44 ± 1.30
1998–2005	-39.64 ± 25.22	-30.29 ± 29.11	-21.95 ± 13.78	-8.73 ± 4.98	2.25 ± 1.19
2006–2008	-33.66 ± 18.50	-90.01 ± 19.11	-18.16 ± 10.72	-5.52 ± 3.64	2.70 ± 1.48

Table 4 also shows the flux of Kinetic Energy. The Ionian imports KE from the Sicily channel and exports it through the Cretan Passage. The highest KE flux is that of the wind, which remains the most important source of KE for the Ionian. Once again the standard deviation of KE flux for the Antikythira strait is higher than all other sources. This flux exhibits again a peak during the EMT phase (not shown).

In order to rank the relevant mechanics driving the vorticity and KE budgets during the different states of circulation previously identified we consider three periods: 1993–1997, 1998–2005 and 2006–2008. The previous results point out the primary importance of Sicily channel as source of KE and vorticity for the Ionian Sea. The exchanges here exhibit an anti-estuarine pattern [*Gacic et al*., 2013; *Cessi et al*., 2014] with AW occupying the upper layers and LIW beneath. As the Sicily channel's inputs of KE and vorticity, does not show substantial variations in OPWIND (not shown), they will not be considered further in our analysis.

Table 5 shows the variation of the vorticity terms from wind stress curl, the stretching term and the flux from Antikythira strait, Otranto strait and Cretan Passage. We limited the analysis of vorticity balance to the first 500 m as the variability in the relative vorticity has been observed mainly there (Figure 6a). During anticyclonic circulation states (Figure 8; 1993–1997 and 2006–2008) stretching is larger than the wind input, which remains prevalent only during the cyclonic state (1998–2005). Again, the stretching term has a negative maximum value during the EMT phase which corresponds timely to a peak, eight times greater than the mean value of flux through the Antikythira Strait. In particular, considering the northern part of the basin (where NIG revereses sign, Figure 4) the wind input is always positive (approximately 8.6 ± 5.48 m^3s^{-2} with a peak during the period 1998–2005 of 9.53 ± 6.32 m^3s^{-2}). In this case, the main input of vorticity for the Northern Ionian comes from the Aegean Sea. The comparison with values observed in the CLWIND experiment (-29.18 ± 22.46 m^3s^{-2}) confirms the importance of nearby basin(s) in driving the vorticity budget of the Ionian [*Borzelli et al*., 2009; *Theocharis et al*., 2014]. Finally, the flux of vorticity through the Otranto Strait does not exhibit significant variations.

Table 6 shows the corresponding analysis for KE. Despite the total KE in the basin does not exhibit strong variations during the three different circulations, the APE_{QG} has two minima during anticyclonic circulation while its value almost doubles during the cyclonic state. The reason for this behavior can be understood by looking at the relative importance of KE variations from wind work and the conversion term APE_{QG}/KE (Figure 9). During anticyclonic states, the main source of KE is represented by the conversion term. APE_{QG} is converted into KE and this explains its minimum values observed and the maximum for KE. This internal mechanism is the main source of KE during the period 1993–1997 and 2006–2008 for the Ionian basin [*Borzelli et al*., 2009; *Gacic et al*., 2010; *Theocharis et al*., 2014] not the wind which, conversely, does not exhibit significant positive peaks . During the period 1998–2005, the conversion APE_{QG}/KE reverts its sign. Wind becomes the main source of KE for the

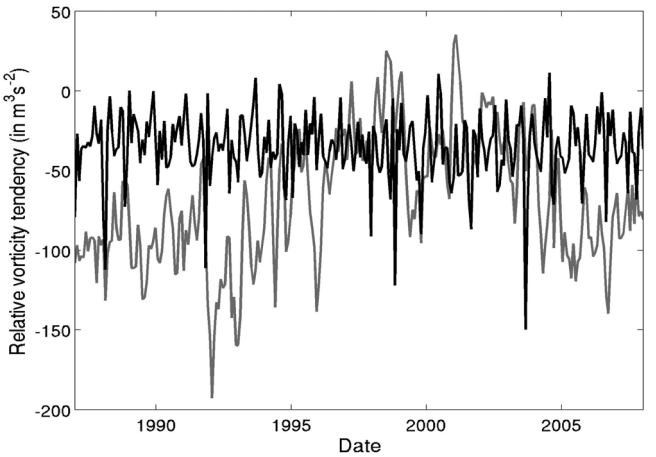

Figure 8. Monthly averaged vorticity tendency (in m^3s^{-2}) due to wind stress curl (black line) and vortex stretching (gray line) in the Ionian Sea (first 500 m) in the period 1987–2008.

Table 6. Flux of KE (Wm^{-3}) From the Wind, Conversion APE_{QG}/KE; Flux of APE_{QG} and KE From Antikythira Strait, Otranto Strait, and Cretan Passage; total KE and APE_{QG} (in J) in the Ionian[a]

	Wind	Conversion APE_{QG}/KE	Antikythira Strait	Otranto Strait	Cretan Passage	Total KE	Total APE_{QG}
1993–1997	$1.69 \times 10^{18} \pm 1.03 \times 10^{18}$	$\mathbf{5.57 \times 10^{18} \pm 6.46 \times 10^{18}}$	$\mathbf{-3 \times 10^{18} \pm 8.24 \times 10^{18}}$ $-1.21 \times 10^{17} \pm 1.92 \times 10^{17}$	$-6.72 \times 10^{17} \pm 1.36 \times 10^{17}$ $1.05 \times 10^{15} \pm 2.05 \times 10^{15}$	$\mathbf{3.55 \times 10^{18} \pm 3.09 \times 10^{18}}$ $3.63 \times 10^{16} \pm 2.35 \times 10^{16}$	$\mathbf{4.91 \times 10^{14} \pm 1.10 \times 10^{14}}$	$5.61 \times 10^{16} \pm 1.29 \times 10^{16}$
1998–2005	$\mathbf{1.94 \times 10^{18} \pm 1.36 \times 10^{18}}$	$-0.24 \times 10^{18} \pm 2.29 \times 10^{18}$	$-3.74 \times 10^{17} \pm 2.32 \times 10^{17}$ $-1.01 \times 10^{16} \pm 7.72 \times 10^{16}$	$\mathbf{4.31 \times 10^{17} \pm 2.88 \times 10^{18}}$ $1.44 \times 10^{15} \pm 1.42 \times 10^{15}$	$7.49 \times 10^{16} \pm 8.81 \times 10^{17}$ $4.46 \times 10^{16} \pm 3.57 \times 10^{16}$	$4.23 \times 10^{14} \pm 1.33 \times 10^{14}$	$\mathbf{9.98 \times 10^{16} \pm 4.41 \times 10^{16}}$
2006–2008	$1.70 \times 10^{18} \pm 0.78 \times 10^{18}$	$\mathbf{5.24 \times 10^{18} \pm 3.56 \times 10^{18}}$	$\mathbf{-6.67 \times 10^{17} \pm 3.67 \times 10^{17}}$ $-2.82 \times 10^{16} \pm 3.17 \times 10^{16}$	$-4.28 \times 10^{17} \pm 6.65 \times 10^{17}$ $1.63 \times 10^{15} \pm 1.832 \times 10^{15}$	$\mathbf{2.53 \times 10^{18} \pm 3.81 \times 10^{18}}$ $3.73 \times 10^{16} \pm 1.35 \times 10^{16}$	$\mathbf{4.59 \times 10^{14} \pm 1.08 \times 10^{14}}$	$7.71 \times 10^{16} \pm 2.09 \times 10^{16}$

[a]The period are 1993–1997, 1998–2005 and 2006–2008.

Ionian basin and KE is converted into APE_{QG}. This explains the increase of APE_{QG} (the buoyancy fluxes are costant throughout the experiment).

Considering the flux of APE_{QG} throughout the boundaries of the basin (Table 6 and Figure 10) the two anticyclonic circulation states are characterized by enhanced exchanges of APE_{QG} between the Ionian and the Antikythira Strait and Cretan Passage corresponding to the onset of the Aegean Sea as the source of deep waters for the Ionian [*Krokos et al.*, 2014; *Theocharis et al.*, 2014; *Velaoras et al.*, 2014]. The cyclonic state corresponds to an enhanced exchange of APE_{QG} with SA (Figure 10), corresponding to the reactivation of SA as the deep waters source toward 1999 [*Krokos et al.*, 2014; *Theocharis et al.*, 2014; *Velaoras et al.*, 2014].

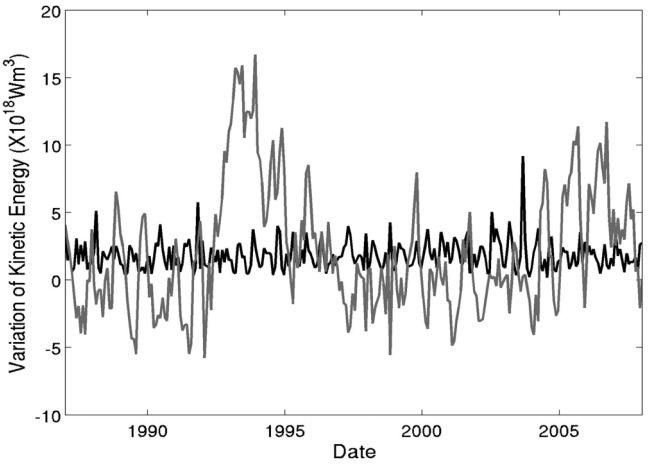

Figure 9. Monthly averaged of kinetic energy tendency (in W m^3) due to wind stress (black line) and conversion APE_{QG}/KE (gray line) in the Ionian in the period 1987–2008.

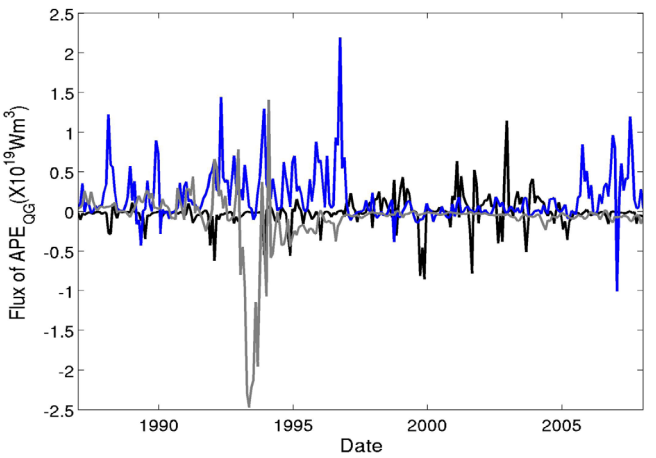

Figure 10. Monthly Flux of APE_{QG} (in Wm^{-3}) through Otranto strait (black line), Antikythira Strait (gray line) and Cretan Passage(blue line) in the period 1987–2008.

4. Discussions and Conclusions

We have used a suite of numerical experiments, of increased complexity in both the domain and forcing, in order to study the baroclinic dynamics of the Adriatic Ionian System. Despite the relative simplicity of the model used, this approach has been able to reproduce the main features of the Ionian Sea circulation in the period 1993–2008.

Our experiments reproduced the different reversals observed in the Ionian Sea in 1997 and 2006 [*Borzelli et al.*, 2009; *Gacic et al.*, 2010; *Bessières et al.*, 2013; *Theocharis et al.*, 2014]. In this framework the wind plays a primary role in the vorticity and kinetic energy budget of the basin [*Korres et al.*, 2000; *Demirov and Pinardi*, 2002; *Molchard et al.*, 2002] but it is not the primary player driving the variability observed [*Gacic et al.*, 2010; *Theocharis et al.*, 2014]. The reversals observed affect the upper layer of the Ionian circulation which exhibits a bi-layer structure. The bottom layer is permanently cyclonic due to the filling of the Ionian with ADW or CDW (Cretan Deep Water). Our analysis has

confermed the role of Ionian Sea in affecting the potential density of the SA [*Gacic et al*., 2010; *Civitarese et al*., 2010].

The main results from our idealized modeling experiments have shown that wind stress role is dominant only in the absence of deep waters formation (DWF) processes in the Aegean Sea and results in a cyclonic circulation [*Pinardi et al*., 1997; *Korres et al*., 2000; *Demirov and Pinardi*, 2002; *Molchard et al*., 2002] in the Northern Ionian while the Southern part of the basin exhibits a permanently anticyclonic circulation. Its role is particularly dominant when considering the flow of vorticity through the Otranto strait.

It has been possible to explain the variability in the vorticity of the upper layer through the vorticity stretching acting on the basin. Changes in the upper layer circulation of the Ionian Sea take place only in presence of an active boundary in the Ionian Sea and Aegean Sea [*Theocharis et al*., 2014] side and it appears to be correlated with substantial exchange of APE_{QG} between these two basins (as observed during the end of the Eastern Mediterranean Transient). These exchanges of APE_{QG} depend strictly on the variability of thermohaline properties of the waters exchanged through the Antikythira Strait and Cretan Passage and have been put in evidence in previous studies [*Krokos et al*., 2014; *Theocharis et al*., 2014; *Velaoras et al*., 2014] and in the analysis of temperature and salinity profiles from the MedArgo project (*Poulain et al.,* 2007). The energetics performed on the system reveals that the AISys reversals can be explained only if the Adriatic-Ionian-Aegean Sea system is explicitly considered, as previously noted in *Theocharis et al*. [2014].

It remains to be investigated whether previous reversals associated with the alternate activation of the Aegean and Adriatic Sea as deep waters sources for the Ionian Sea have indeed happened. This will be analyzed with recent advanced hindcast simulations for the AISys in coupled and uncoupled mode in a future study.

Appendix A

MITgcm is a state of the art three-dimensional model that can be used to simulate, on a wide range of computational platforms, the dynamics of the atmosphere and the ocean in a wide range of spatial and temporal scales [*Adcroft et al*., 1997; *Marshall et al*., 1997a,1997b]. The MITgcm employs a finite volume approach to discretize the momentum equations and the partial cells to treat complex geometries.

Assuming an incompressible flow and the Boussinesq approximation, the equations solved by MITgcm are [*Adcroft et al*., 1997; *Marshall et al*., 1997a,1997b]:

Momentum:

$$\rho_o D_t \vec{u} + 2\rho_o \Omega \times \vec{u} + g\rho_o \vec{k} + \vec{\nabla} p = \vec{F} \tag{A1}$$

Continuity:

$$\rho_o \nabla \cdot \vec{u} = 0 \tag{A2}$$

Mass Conservation:

$$\partial_t \eta + \nabla \cdot (H+\eta)\vec{u}_h = \mathrm{Pr} - Ev + Runoff \tag{A3}$$

Energy Conservation:

$$D_t T = A_T \nabla^2 T + Q_T \tag{A4}$$

Salt Conservation:

$$D_t S = A_S \nabla^2 S + Q_S \tag{A5}$$

Equation of state:

$$\rho = \rho(S, p, T) \tag{A6}$$

where $\vec{u}$ is the three dimensional velocity vector, p is pressure, ρ is in-situ density, η is the displacement of the free-surface from the sea level at the rest, T is the potential temperature and S is salinity, ρ_o is a constant reference density, g is the constant gravitational acceleration and H is a fixed-in-time bottom depth [*Adcroft et al*., 1997; *Marshall et al*., 1997a,1997b]. $\vec{F}$ (including wind and dissipation terms), Pr-Ev+Runoff, Q_T, and Q_S

are the forcing fields. $\nabla^2 T$ and $\nabla^2 S$ are the diffusive fluxes of heat and salt, A_T and A_S are the horizontal eddy diffusive coefficients for the temperature and salinity. D is the material operator $(\partial_t + u \cdot \nabla)$

MITgcm uses the hydrostatic approximation in the vertical momentum equation [*Adcroft et al.*, 1997; *Marshall et al.*, 1997a,1997b]. The equations are integrated in space over space-filling finite volumes (cells) and in time according to a quasi-second order Adams-Bashfort scheme. The resulting horizontal velocities components are staggered on a Arakawa C-grid while the vertical component on a Lorenz grid.

Appendix B

Assuming a two dimensional flow $\vec{u}_h$ where the hydrostatic approximation holds the momentum equations are:

$$\rho D_t \vec{u}_h + 2\rho\vec{\Omega}\times\vec{u}_h + g\rho\vec{k} + \vec{\nabla}p = \frac{\vec{\tau}}{H} + \mu\nabla^2\vec{u}_h \tag{B1}$$

where $\vec{\tau}$ is the wind stress (in N/m^2), μ is the dinamical viscosity (in m/s^2), $\nabla^2\vec{u}_h$ is the laplacian of horizontal velocity and H is the thickness of the layer of the fluid (e.g., 500 m). The numerical equivalent for the momentum budget can be established using the different diagnostics provided by the model, which mainly reflects the time-stepping options. The momentum balance for the zonal component of the velocity (u*) can be written as:

$$\partial_t u^* = -g\frac{\partial\eta*}{\partial x} + u^{**}_{hydrostatic-pressure} + u^{**}_{advection} + u^{**}_{coriolis} + u^{**}_{diffusion} + u^{**}_{external-forcings} + u^{**}_{viscous-vertical-flux} \tag{B2}$$

Equation (B2) shows that temporal variations of u* are given by the sum of variations (u**, right hand side of the equation) of u* induced by surface pressure gradient, hydrostatic horizontal pressure gradient, advection, Coriolis force, viscous diffusion, external forcing (such as wind) and vertical viscous flux of momentum. $\eta*$ is the numerical sea surface height anomaly and g is the gravitational acceleration. The same balance holds for v*, the meridional component of the velocity. All the quantities on both sides are provided by the model except for the tendency from sea surface height and vertical viscous fluxes.

Applying the curl operator to (B1) we obtain the well-known Vorticity Balance:

$$\partial_t\varsigma = (\varsigma\cdot\nabla)\vec{u}_h - \varsigma\nabla\cdot\vec{u}_h - (\vec{u}_h\cdot\nabla)\varsigma + \frac{\nabla\rho\times\nabla p}{\rho^2} + \frac{\nabla\times\vec{\tau}}{\rho H} + \upsilon\nabla^2\varsigma \tag{B3}$$

where the temporal variation of the relative vorticity (ς), equivalent to the vorticity previously considered (in s^{-1}), in a point is given by tilting and stretching/squeezing of water column, advection of the vorticity, baroclinicity, input from wind stress and diffusion of vorticity. The corresponding vorticity balance using the MITgcm output can be found applying the curl as discretized in the model:

$$\frac{1}{A_\varsigma}(\delta_i\Delta y_c v^* - \delta_j\Delta x_c u^*) \tag{B4}$$

where A_ς is the area of vorticity cell, $\delta_j\Delta x_c u^*$ is equal to $v^*_i\cdot\Delta y_{c_i} - v^*_{i-1}\cdot\Delta y_{c_{i-1}}$ and $\delta_j\Delta x_c u^*$ is equal to $u^*_j\cdot\Delta x_{c_j} - u^*_{j-1}\cdot\Delta x_{c_{j-1}}$. $\Delta y_c, \Delta x_c$ are respectively the distance between the centers of the cell along the x and y direction respectively. Each quantity is computed over the first 500 m (as the variation in the circulation has been observed over those depths). Mean quantitities are computed over the period 1987–2008 and are expressed in m^{3}s^{-2}. The reason for choosing these units of measure derives from the need of comparing these quantities with vorticity inflow through the boundaries of the Ionian domain. We define as zonal vorticity flux through the boundaries (Strait of Otranto, Sicily channel etc) the following quantity:

$$\int\int u\cdot\zeta dxdz \tag{B5}$$

The same definition holds for the meridional vorticity flux. The only limit of these definition is that we cannot derive informations about the direction of this flux (vorticity can be either positive or negative).

Multiplying (B1) by u_h and taking the scalar product we find the equation for the temporal variation of KE (in J):

$$\partial_t KE = -u_h\nabla p + \frac{\tau u}{H} + \upsilon\nabla^2 KE \tag{B6}$$

where the first term on the rhs represents the conversion from APE_{QG} to KE, the second the energy input from the wind and the third the dissipation of KE.

APE_{QG} is that part of the potential energy that can be potentially transformed into kinetic energy through mechanisms concerning either barotropic or baroclinic instabilities [*Korres et al.*, 2000]. APE_{QG} can be defined as [*Huang*, 2005; *Brown et al.*, 2011]:

$$-g\iiint_V \frac{[\rho-\bar{\rho}(z)]^2}{2\rho_z}dxdydz \tag{B7}$$

where ρ is the local potential density, $\bar{\rho}(z)$ the averaged potential density at any given level (which represents the reference state) and $\bar{\rho}_z$ the vertical local gradient of potential density.

The numerical equivalent to (B6) can be found multiplying (B2) for u*, and the meridional component for v*, and summing. The equivalent temporal variation of kinetic energy in the model (KE*) is given by:

$$KE_t{}^* = KE^{**}{}_{ssh} + KE^{**}{}_{conversionAPE/KE} + KE^{**}{}_{advection} + KE^{**}{}_{coriolis} + KE^{**}{}_{diffusion} + KE^{**}{}_{wind} + KE^{**}{}_{viscous\text{-}vertical\text{-}flux} \tag{B8}$$

In this numerical balance the temporal variation of KE* is given by surface pressure gradient, conversion APE_{QG}/KE, advection, Coriolis force, viscous diffusion, external forcings (wind) and vertical viscous flux. It is worthwhile mentioning that, because of numerical reasons, the Coriolis term is not necessarily zero in the model, whereas it obviously has a null contribution to the analitycal expression. Each quantity of the balance are mean quantities for the period 1987–2008 and will be expressed in W m^{-3} over the entire water column in order to compare these quantities with the exchanges of energy between Ionian Sea and nearby basins. We define the flux of KE and APE_{QG} through the boundaries respectively as [*Cessi et al.*, 2014]

$$\iint KE \cdot udxdz \tag{B9}$$

$$\iint APE_{QG} \cdot udxdz \tag{B10}$$

The direction of the flow in this case is pointed out by the zonal/meridional component of speed.

Acknowledgments
The authors would like to express their gratitude to S. Querin and G. Sannino for their technical support in using the MITgcm model; M. Gacic and G. Civitarese for the discussion about BiOS, J.M Campin and F. Falcioni for their useful suggestions about momentum and vorticity budgets in MITgcm. The authors are also deeply grateful to L. Mariotti, S. Bacer, A.Fantini and E. Coppola (coppolae@ictp.it) for providing, upon request, wind data from RegCM4 simulations and W.Roether (wroether@physik.uni-bremen.de) for providing, upon request, temperature and salinity data of the German Cruises M5/6, M31/1, M44/4 and M52/2. We are deeply grateful to Meteo-France/CNRM, S.Somot (samuel.somot@meteo.fr) and F.Sevault for running and providing upon request the NEMOMED8 simulation data. The authors acknowledge the European project MyOcean for the reanalysis data of currents for the period 1987–2012 avalaible at http://marine.copernicus.eu/. M.Reale would like to thank Ekin Akoglu for the discussions about coupling and Kelvin waves and P.Lionello for the kind hospitality offered during the last part of this work.The authors are greatful to V. Artale for his useful comments and suggestions during the final stages of this work. This work has been partially supported by the Italian flagship program RITMARE. M. Reale in the last stage of the work was supported by OGS and CINECA under HPC-TRES program award number 2015-07.

References

Adcroft, A., C. Hill, and J. Marshall (1997), The representation of topography by shaved cells in a height coordinate model, *Mon. Weather Rev.*, *125*(9), 2293–2315.

Bensi, M., Velaoras, D., V. L. Meccia, and V. Cardin (2016), Effects of the Eastern Mediterranean Sea circulation on the thermohaline properties as recorded by fixed deep-ocean observatories, *Deep Sea Res., Part I*, *112*, 1-13.

Bessières, L., M. H. Rio, C. Dufau, C. Boone, and M. I. Pujol (2013), Ocean state indicators from MyOcean altimeter products, *Ocean Sci.*, *9*, 545–560.

Beuvier, J., F. Sevault, M. Herrmann, H. Kontoyiannis, W. Ludwig, M. Rixen, E. Stanev, K. Béranger, and S. Somot (2010), Modeling the Mediterranean Sea interannual variability during 1961–2000: Focus on the Eastern Mediterranean Transient, *J. Geophys. Res.*, *115*, C08017, doi:10.1029/2009JC005950.

Borzelli, G. L. E., M. Gacic, V. Cardin, and G. Civitarese (2009) Eastern Mediterranean Transient and reversal of the Ionian Sea circulation, *Geophys. Res. Lett.*, *36*, L15108, doi:10.1029/2009GL039261.

Brown J, A. Fedorov, and E. Guilyardi (2011), How Well do coupled models replicate ocean energetics relevant to Enso, *Clim. Dyn.*, *36*, 2147–2158.

Cardin, V., G. Civitarese, D. Hainbucher, M. Bensi, and A. Rubino (2014), Thermohaline properties in the Eastern Mediterranean in the last three decades: Is the basin returning to the pre-EMT situation?, *Ocean Sci. Discuss.*, *11*(1), 391–423, doi:10.5194/osd-11-391-2014.

Cessi, P., N. Pinardi, and V. Lyubartsev (2014), Energetics of semienclosed basins with two-layer flows at the strait, *J. Phys. Oceanogr.*, *44*, 967–979.

Civitarese, G., M. Gačić, M. Lipizer, and G. L. Eusebi Borzelli (2010), On the impact of the Bimodal Oscillating System (BiOS) on the biogeochemistry and biology of the Adriatic and Ionian Seas (Eastern Mediterranean), *Biogeosciences*, *7*, 3987–3997, doi:10.5194/bg-7-3987-2010.

Demirov, E., and N. Pinardi (2002), Simulation of the Mediterranean Sea circulation from 1979 to 1993: Part I. The interannual variability, *J. Mar. Syst.*, *33–34*, 23-50.

Gacic, M., A. Lascaratos, B. Manca, and A. Mantziafou (2002), *Adriatic deep water and interaction with the Eastern Mediterranean Sea, in Physical Oceanography of the Adriatic Sea. Past, Present and Future*, edited by B. Cushman-Roisin, et al., chap. 4, pp. 111–142, Kluwer Acad., Springer, Dordrecht, Netherlands.

Gacic, M., G. L. E. Borzelli, G. Civitarese, V. Cardin, and S. Yari (2010), Can internal processes sustain reversals of the ocean upper circulation? The Ionian Sea example, *Geophys. Res. Lett.*, *37*, L09608, doi:10.1029/2010GL043216.

Gacic, M., G. Civitarese, G. L. Eusebi Borzelli, V. Kovacevic, P.-M. Poulain, A. Theocharis, M. Menna, A. Catucci, and N. Zarokanellos (2011), On the relationship between the decadal oscillations of the northern Ionian Sea and the salinity distributions in the eastern Mediterranean, *J. Geophys. Res.*, *116*, C12002, doi:10.1029/2011JC007280.

Gacic, M., K. Schroeder, G. Civitarese, S. Cosoli, A. Vetrano, and G. L. Eusebi Borzelli (2013), Salinity in the Sicily Channel corroborates the role of the Adriatic-Ionian Bimodal Oscillating System (BiOS) in shaping the decadal variability of the Mediterranean overturning circulation, *Ocean Sci.*, *9*(1), 83–90.

Gacic, M., et al. (2014), Extreme winter 2012 in the Adriatic: An example of climatic effect on the BiOS rhythm, *Ocean Sci.*, *10*, 513–522, doi: 10.5194/os-10-513-2014.
Gill, A., J. Green, and A. Simmons (1974), Energy partition in the large-scale ocean circulation and the production of mid-ocean eddies, *Deep Sea Res. Oceanogr. Abstr.*, *21*(7), 499–528, doi:10.1016/0011-7471(74)90010-2.
Giorgi, F., et al. (2012), RegCM4: Model description and preliminary tests over multiple CORDEX domains, *Clim. Res.*, *52*, 7–29.
Gunduz, M., S. Dobricic, P. Oddo, N. Pinardi, and A. Guarnieri (2013), Impact of Levantine Intermediate Water on the interannual variability of the Adriatic Sea based on simulations with a fine resolution ocean model, *Ocean Modell.*, *72*, 253–263, doi:10.1016/j.ocemod.2013.10.002.
Herrmann, M., F. Sevault, J. Beuvier, and S. Somot (2010), What induced the exceptional 2005 convection event in the northwestern Mediterranean basin? Answers from a modeling study, *J. Geophys. Res.*, *115*, C12051, doi:10.1029/2010JC006162.
Huang, R. X. (2005), Available potential energy in the world's oceans, *J. Mar. Res.*, *63*, 141–158.
Klein, B., W. Roether, B. Manca, D. Bregant, V. Beitzel, V. Kovacevic, and A. Luchetta (1999), The large deep-water transient in the Eastern Mediterranean, *Deep Sea Res., Part I*, *46*, 371–414.
Klein, B., W. Roether, G. Civitarese, M. Gacic, B. B. Manca, and M. Ribera D'alcala (2000), Is the Adriatic returning to dominate the production of Eastern Mediterranean Deep Water?, *Geophys. Res. Lett.*, *27*, 3377–3380.
Kontoyiannis, H., A. Theocharis, E. Balopoulos, S. Kioroglou, V. Papadopoulos, M. Collins, A. F. Velegrakis, and A. Iona (1999), Water fluxes through the Cretan Arc Straits, Eastern Mediterranean Sea: March 1994 to June 1995, *Prog. Oceanogr.*, *44*, 511-529.
Korres G., N. Pinardi, and A. Lascaratos (2000), The ocean response to low-frequency interannual atmospheric variability in the Mediterranean Sea. Part I: Sensitivity experiments and energy analysis, *J. Clim.*, *13*, 705–731.
Krokos, G., D. Velaoras, G. Korres, L. Perivoliotis, and A. Theocharis (2014), On the continuous functioning of an internal mechanism that drives the Eastern Mediterranean thermohaline circulation: The recent activation of the Aegean Sea as a dense water source area, *J. Mar. Syst.*, *129*, 484–489, doi:10.1016/j.jmarsys.2013.10.002.
Large, W. G., J. C. McWilliams, and C. S. Doney (1994), Oceanic vertical mixing: A review and a model with nonlocal boundary layer parameterization, *Rev. Geophys.*, *32*, 363–403.
Lascaratos, A., W. Roether, K. Nittis, and B. Klein (1999), Recent changes in the deep-water formation and spreading in the Eastern Mediterranean, *Prog. Oceanogr.*, *44*(1-3), 5–36.
Lipizer, M., E. Partescano, A. Rabitti, A. Giorgetti, and A. Crise (2014), Qualified temperature, salinity and dissolved oxygen climatologies in a changing Adriatic Sea: Ocean Science, vol. 10, pp. 771–797.
Manca, B. B., V. Kovacevic, M. Gacic, and D. Viezzoli (2002), Dense water formation in the Southern Adriatic sea and spreading into the Ionian Sea in the period 1997-1999, *J. Mar. Syst.*, *33-34*, 133–154.
Mantziafou, A., and A. Lascaratos (2004), An eddy resolving numerical study of the general circulation and deep-water formation in the Adriatic Sea, *Deep Sea Res., Part I*, *51*(7), 251–292.
Mantziafou, A., and A. Lascaratos (2008), Deep-water formation in the Adriatic Sea:Interannual simulations for the years 1979-1999, *Deep Sea Res., Part I*, *55*, 1403–1427.
Marshall, J., A. Adcroft, C. Hill, L. Perelman and C. Heisey (1997a), A finite-volume, incompressible Navier Stokes model for studies of the ocean on parallel computers, *J. Geophys. Res. 102*, 5753–5766.
Marshall, J., C. Hill, L. Perelman, C. Heisey, and A. Adcroft (1997b), Hydrostatic, quasi-hydrostatic and nonhydrostatic ocean modeling, *J. Geophys. Res.*, *102*, 5733–5752.
Molchard, A., N. Pinardi, M. Iskandararni, and D. B. Haidvogel (2002), Wind driven general circulation of the Mediterranean Sea simulated with a Spectral Element Ocean Model, *Dyn. Atmos. Oceans*, *35*, 97–130.
Nittis, K. N. Pinardi and A. Lascaratos (1993), Characteristics of the summer 1987 flow field in the Ionian Sea, *J. Geophys. Res.*, *98*(C6), 10171–10184, doi:10.1029/93JC00451.
Oddo, P., M. Adani, N. Pinardi, C. Fratianni, M. Tonani, and D. Pettenuzzo (2009), A nested Atlantic-Mediterranean Sea general circulation model for operational forecasting, *Ocean Sci.*, *5*, 461–473, doi:10.5194/os-5-461-2009.
Pinardi, N., G. Korres, A. Lascaratos, V. Roussenov, and E. Stanev (1997), Numerical simulation of the interannual variability of the Mediterranean Sea upper ocean circulation, *Geophys. Res. Lett.*, *24*, 425–428.
Poulain, P., et al. (2007), MedArgo: A drifting profiler program in the Mediterranean Sea, *Ocean Sci.*, *3*(3), 379–395.
Querin, S., A. Crise, D. Deponte, and C. Solidoro (2006), Numerical study of the role of wind forcing and freshwater buoyancy input on the circulation in a shallow embayment (Gulf of Trieste, Northern Adriatic Sea), *J. Geophys. Res.*, *111*, C03S16, doi:10.1029/2006JC003611.
Roether, W., B. Manca, B. Klein, D. Bregant, D. Georgopoulos, V. Beitzel, V. Kovacevic, and A. Luchetta (1996), Recent changes in the Eastern Mediterranean deep waters, *Science*, *271*, 333–335.
Roether, W., B. Klein, B. Manca, A. Theocharis, and S. Kioroglou (2007), Transient Eastern Mediterranean deep waters in response to the massive dense-water output of the Aegean Sea in the 1990s, *Prog. Oceanogr.*, *74*, 540–571.
Ruti, P., et al. (2014), MED-CORDEX initiative for Mediterranean Climate studies, submitted to Bulletin of American Meteorological Society, doi:10.1175/BAMS-D-14-00176.1.
Sayin, E., and T. Besiktepe (2010), Temporal evolution of the water mass properties during the Eastern Mediterranean transient (EMT) in the Aegean Sea, *J. Geophys. Res.*, *115*, C10025, doi:10.1029/2009JC005694.
Schroeder, K., et al. (2012), Circulation of the Mediterranean Sea and its variability, in *The Climate of the Mediterranean Region. From the Past to the Future*, edited by P. Lionello, pp. 187–256, Elsevier, Amsterdam.
Theocharis, A., K. Nittis, H. Kontoyiannis, E. Papageorgiou, and E. Balopoulos (1999), Climatic changes in the Aegean Sea influence the Eastern Mediterranean thermohaline circulation, *Geophys. Res. Lett.*, *26*, 1617–1620.
Theocharis, A., B. Klein, K. Nittis, and W. Roether (2002), Evolution and status of the East Mediterranean transient (1997-1999), *J. Mar. Syst.*, *33*, 91–116.
Theocharis, A., G. Krokos, D. Velaoras and G. Korres (2014), An internal mechanism driving the alternation of the Eastern Mediterranean dense/deep water sources, in *The Mediterranean Sea: Temporal Variability and Spatial Patterns, AGU Geophys. Monogr. Ser., 202*, edited by G. L. E. Borzelli *et al*., chap. 8, pp. 113–137, John Wiley, Oxford, U. K., doi:10.1002/9781118847572.
Velaoras, D., G. Krokos, K. Nittis, and A. Theocharis (2014), Dense intermediate water outflow from the Cretan Sea: A salinity driven, recurrent phenomenon, connected to thermohaline circulation changes, *J. Geophys. Res. Oceans*, *119*, 4797–4820, doi:10.1002/2014JC009937.